CrossMark

Lattice hydrodynamic model for traffic flow on curved road with passing

Yue-Dan Jin · Jie Zhou (iD) **· Zhong-Ke Shi · Hai-Liang Zhang · Chao-Ping Wang**

Abstract In order to investigate the effect of passing upon traffic flow on curved road, in this paper, an extended one-dimensional lattice hydrodynamic model for traffic flow on curved road with passing is proposed. The stability condition is obtained by the use of linear stability analysis. The result of stability analysis shows that passing behavior plays an important role in influencing the stability of traffic flow as well as radian of curved road. The nonlinear wave equations including Burgers, Korteweg-de Vries and modified Korteweg-de Vries equations are derived to describe the nonlinear traffic behavior in different regions, respectively. The analytical results show that reducing the coefficient of passing may enhance the stability of traffic flow. Jamming transition occurs between uniform flow and kink jam when the coefficient of passing is less than the critical value. When the coefficient of passing is larger than the critical value, jamming transition occurs from uniform flow to irregular wave through chaotic phase with decreasing sensitivity parameter. In addition, compared with other segments of curved road, traffic flow with passing easily becomes unstable and complicated at the entrance and exit of curved road, especially at the entrance of curved road. The numerical simulations are given to illustrate and clarify the analytical results.

Keywords Traffic flow · Nonlinear analysis · Chaotic jam · Curved road

1 Introduction

Because of the highly correlated with human life, traffic flow and its related problem, which can been seen as physical phenomena [1–5], have been widely investigated by using different methodologies [6–62]. A series of experiments had been done for investigating the mechanism of traffic flow and identifying the influencing factors [14–17]. Many interesting non-equilibrium phenomena such as phase transition, density waves, stop-and-go flows, local clusters and ghost jams had been observed. In order to make a better understanding and give a well explanation for traffic flow, there is a demand for realistic and quantitative models that can duplicate the phenomena observed in a real situation and explain the evolution mechanism of phase transition. To achieve this goal, various traffic flow models including the continuum models [6–13], car-following models [20–30], and lattice hydrodynamic models [31–62] were proposed by many scholars with different backgrounds.

Y.-D. Jin · J. Zhou (✉) · H.-L. Zhang · C.-P. Wang
School of Mathematics, Physics and Information Science,
Zhejiang Ocean University, Zhoushan 316022, China
e-mail: zhoujie@zjou.edu.cn

Y.-D. Jin · J. Zhou · H.-L. Zhang · C.-P. Wang
Key Laboratory of Oceanographic Big Data Mining and
Application of Zhejiang Province, Zhoushan 316022,
Zhejiang, China

J. Zhou · Z.-K. Shi
College of Automation, Northwestern Polytechnical University,
Xi'an 710072, Shaanxi, China

Lattice hydrodynamic model, which was deduced based on the car-following models and the continuum models, was firstly proposed by Nagatani in Ref. [33]. By using the linear stability theory and nonlinear analysis method, Nagatani found the neutral stability line and the modified Korteweg-de Vries (MKdV) equation successfully, and derived the solutions of kink density wave in the MKdV. Based on the model proposed by Nagatani, many researchers had proposed many extended versions with the consideration of different factors like anticipation effect [42,48,49], driver's characteristics [40,50,53,54], forward and backward looking effect [44,57], traffic interruption probability [41,51], and (multiply) density difference effect [47,55,56]. Passing behavior, as one of the inevitable but dangerous driving behaviors, had been investigated by some scholars. In Ref. [37], Nagatani proposed an extended lattice model considering the effect of passing and found that passing has an important effect on traffic flow. Gupta and Redhu [38] proposed an new lattice model considering driver's anticipation behavior with passing effect and found that traffic jam can be suppressed efficiently by considering the anticipation effect. The result revealed that the negative effect of passing upon traffic flow can be alleviated by taking anticipation effect into account. Furthermore, Gupta et al. [39] proposed a lattice model to investigate the effect of multi-phase optimal velocity function upon traffic flow with passing and concluded that the proposed model can significantly enhance the stability of traffic flow for any value of passing constant even in the case of multi-phase optimal velocity model. In Ref. [40], the effect of driver's characteristics on traffic flow with passing had been investigated. However, to our knowledge, the effect of road condition upon traffic flow with passing has not been discussed until now.

In general, traffic is a combination of people, vehicles, and roads. As the implementation of traffic infrastructure, road is an important influence factor on traffic flow. Considering road situation, Tang et al. [24] proposed a car-following model to investigate the effect of road conditions on traffic flow. Zhu and Zhang [60] proposed a lattice model considering the effect of gradient. In Ref. [62], Zhou and Shi investigated the effects of radian and angle going into curved road on traffic flow by using an extended lattice hydrodynamic model; the results showed that these two factors had an important influence on the stability of traffic flow. From the results, we can see traffic flow on curved road

is more complicated than the one on straight highway. And it deserves further study by considering other factors. Passing, as we know, is a significant factor which greatly affect the stability and safety of traffic flow on curved road. Considering traffic safety, passing is prohibited when vehicles running on curved road especially sharp turn. But with the development of road construction, there exists multi-lane traffic system in modern traffic. In addition, aggressive drivers tend to overtake when passing conditions are satisfied even on curved road. Hence, we propose an extended lattice model to study the effect of passing on traffic flow on curved road.

The paper is organized as follows. In Sect. 2, the model is formulated by considering passing behavior for traffic flow on curved road. The stability analysis is obtained by using linear stability analysis in Sect. 3. We can see the stability condition varies with the parameter of passing γ. In Sect. 4, the Burgers, Korteweg-de Vries (KdV), and MKdV equations are derived in three types of traffic flow regions by using nonlinear analysis. The simulations are given in Sect. 5. Section 6 is the summary.

2 Model

In Ref. [62], Zhou and Shi proposed a lattice hydrodynamic model to investigate traffic flow on curved road. The model is

$$\partial_t \rho(j, t) + \frac{\rho_0}{\sin \theta_j} \partial_j \rho(j, t) v(j, t) = 0, \tag{1}$$

with the following evolution equation of traffic flux ρv at site j

$$\rho(j, t + \tau) v(j, t + \tau) = \frac{\rho_0}{\sin \theta_j} V(\rho(j + 1, t)), \tag{2}$$

where θ_j represents the radian at site j of the curved road. ρ_0 is the total average density. $\rho(j, t)$, $v(j, t)$ denote the density and velocity at site j at time t, respectively. $V(\rho(j, t))$ is the optimal velocity function. Here we select $V(\rho(j, t))$ as follows [62]

$$V(\rho(j, t)) = k \frac{\sqrt{\mu g R}}{2} \left\{ \tanh \left[\frac{2}{\rho_0} - \frac{\rho(j, t)}{\rho_0^2} - \frac{1}{\rho_c} \right] \right.$$
$$\left. + \tanh \left(\frac{1}{\rho_c} \right) \right\}, \tag{3}$$

where ρ_c is the critical density and it is equal to the inverse of the safety distance [50]. R is the radius of

curved road, g is gravity acceleration. k is the control parameter of $v_{\max}$. Because when running on curved road, drivers always slow down with the consideration of safety, the velocity is far less than the maximal velocity.

In terms of Nagatani's idea [37], passing occurs when the traffic current on site j is larger than the one on site $j + 1$. It is assumed that the traffic quantity of the passing on site j is proportional to the difference between the optimal traffic currents on sites j and $j+1$. Hence, we modify the evolution Eq. (2) by taking passing effect into account, that is

$$
\begin{aligned}
&\rho(j, t + \tau) v(j, t + \tau) \\
&= \frac{\rho_0}{\sin \theta_j} V(\rho(j + 1, t)) + \frac{\gamma \rho_0}{\sin \theta_j} \\
&\quad \times [V(\rho(j + 1, t)) - V(\rho(j + 2, t))].
\end{aligned}
\tag{4}
$$

Here γ is the parameter of passing.

By inserting Eq. (4) into Eq. (1), and when site j is sufficiently close to site $j - 1$, then $\theta_j \approx \theta_{j-1}$. The total density equation is obtained as

$$
\begin{aligned}
&\rho(j, t + 2\tau) - \rho(j, t + \tau) \\
&+ \frac{\tau \rho_0^2}{\sin^2 \theta_j} [V(\rho(j + 1, t)) - V(\rho(j, t))] \\
&- \frac{\gamma \tau \rho_0^2}{\sin^2 \theta_j} [V(\rho(j + 2, t)) - 2V(\rho(j + 1, t)) \\
&+ V(\rho(j, t))] = 0.
\end{aligned}
\tag{5}
$$

3 Linear stability analysis

We apply the linear stability theory to analyze the traffic flow model described by Eq. (5). Supposing the vehicles running on curved road with the uniform density ρ_0 and optimal velocity $V(\rho_0)$, then we get the uniform steady state solution $\rho(j, t)$ for Eq. (5)

$$
\rho(j, t) = \rho_0, v(j, t) = V(\rho_0).
\tag{6}
$$

Assuming $y(j, t)$ be a small deviation from the uniform steady solution, that is

$$
\rho(j, t) = \rho_0 + y(j, t).
\tag{7}
$$

Inserting it and Eq. (6) into Eq. (5), then the linearized equation for $y(j, t)$ is obtained from Eq. (5)

$$
\begin{aligned}
&y(j, t + 2\tau) - y(j, t + \tau) \\
&+ \frac{\tau \rho_0^2}{\sin^2 \theta_j} V'(\rho_0)[y(j + 1, t) - y(j, t)] \\
&- \frac{\gamma \tau \rho_0^2}{\sin^2 \theta_j} V'(\rho_0)[y(j + 2, t) \\
&- 2y(j + 1, t) + y(j, t)] = 0,
\end{aligned}
\tag{8}
$$

where $V'(\rho_0)$ is the derivative of optimal velocity function $V(\rho)$ at point $\rho = \rho_0$. Expand $y(j, t) \propto \exp[ikj + zt]$ resulting in the following equation of z

$$
\begin{aligned}
&e^{2z\tau} - e^{z\tau} + \frac{\tau \rho_0^2}{\sin^2 \theta_j} V'(\rho_0)(e^{ik} - 1) \\
&+ \frac{\gamma \tau \rho_0^2}{\sin^2 \theta_j} V'(\rho_0)(2e^{ik} - e^{2ik} - 1) = 0,
\end{aligned}
\tag{9}
$$

where $z = z_1(ik) + z_2(ik)^2 + \cdots$, and inserts it into Eq. (9), the first- and second-order terms of ik are obtained

$$
z_1 = -\frac{\rho_0^2}{\sin^2 \theta_j} V'(\rho_0),
\tag{10}
$$

$$
z_2 = -\frac{3\tau \rho_0^4 V'^2(\rho_0)}{2\sin^4 \theta_j} - \frac{(1 - 2\gamma)\rho_0^2 V'(\rho_0)}{2\sin^2 \theta_j}.
\tag{11}
$$

If $z_2 > 0$, the uniform steady state becomes stable, while the uniform steady state becomes unstable if $z_2 < 0$. Then the stable condition for traffic flow is

$$
\tau < \frac{-(1 - 2\gamma)\sin^2 \theta_j}{3\rho_0^2 V'(\rho_0)}.
\tag{12}
$$

Moreover, for small disturbances of long wave length, the neutral stability condition is given by

$$
\tau_s = \frac{-(1 - 2\gamma)\sin^2 \theta_j}{3\rho_0^2 V'(\rho_0)}.
\tag{13}
$$

When $\theta_j = \pi/2$, the results are agreed with the ones in Ref. [37]. When $\gamma = 0$, the results are agreed with the ones in Ref. [62].

The neutral stability lines (solid lines) in the space (ρ, a) ($a = 1/\tau$) for different values of γ with $\rho_0 = \rho_c = 0.2, \theta_j = \pi/4, \mu = 0.3, R = 20, k = 0.14$ are shown in Fig. 1. The region, which is within the neutral stability line, is the unstable region. The apex of each curve represents the critical point (ρ_c, a_c). From Fig. 1, it is shown that the unstable region enlarges with increasing γ, which means traffic flow becomes unstable with the increasing of γ.
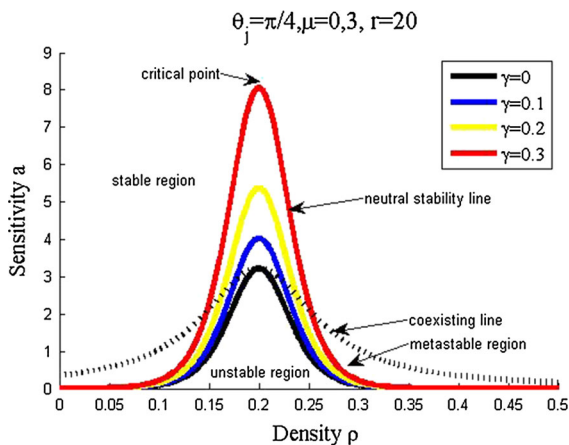
Fig. 1 Phase diagram in the (ρ, a) space with $\rho_0 = \rho_c = 0.2$, $\mu = 0.3$, $R = 20$, $k = 0.14$ for different γ

4 Nonlinear analysis

In this section, we study the nonlinear behavior of traffic flow described by Eq. (5). Note that the Eq. (5) is a nonlinear partial differential equation, and it is difficult to get the exact and analytical solution for Eq. (5). To overcome this difficulty, we apply the reductive perturbation method introduced in Ref. [38] to solve Eq. (5). We introduce slow scales for space variable j and time variable t and define slow variables X and T for $0 < \varepsilon \ll 1$ [57]

$$X = \varepsilon(j + bt), \qquad T = \varepsilon^s t \tag{14}$$

where b is a constant to be determined. Assuming

$$\rho(j, t) = \rho_0 + \varepsilon^l R(X, T). \tag{15}$$

By substituting Eqs. (14)–(15) into Eq. (5) and expanding to the $s + l + 1$ order of ε, we obtain the following nonlinear partial differential equation

$$
\begin{aligned}
&\varepsilon^{l+1}\Big[b + \frac{\rho_0^2 V'(\rho_0)}{\sin^2 \theta_j}\Big]\partial_X R \\
&+ \varepsilon^{l+2}\Big[\frac{3b^2\tau}{2} + \frac{(1-2\gamma)\rho_0^2 V'(\rho_0)}{2\sin^2 \theta_j}\Big]\partial_X^2 R \\
&+ \varepsilon^{l+3}\Big[\frac{7b^3\tau^2}{6} + \frac{(1-6\gamma)\rho_0^2 V'(\rho_0)}{6\sin^2 \theta_j}\Big]\partial_X^3 R \\
&+ \varepsilon^{l+4}\Big[\frac{5b^4\tau^3}{8} + \frac{(1-14\gamma)\rho_0^2 V'(\rho_0)}{24\sin^2 \theta_j}\Big]\partial_X^4 R \\
&+ \varepsilon^{2l+1}\frac{\rho_0^2 V''(\rho_0)}{2\sin^2 \theta_j}\partial_X R^2 + \varepsilon^{2l+2}\frac{(1-2\gamma)\rho_0^2 V''(\rho_0)}{4\sin^2 \theta_j}\partial_X^2 R^2 \\
&+ \varepsilon^{3l+1}\frac{\rho_0^2 V'''(\rho_0)}{6\sin^2 \theta_j}\partial_X R^3
\end{aligned}
\tag{16}
$$

$$
\begin{aligned}
&+ \varepsilon^{3l+2}\frac{(1-2\gamma)\rho_0^2 V'''(\rho_0)}{12\sin^2 \theta_j}\partial_X^2 R^3 \\
&+ \varepsilon^{s+l}\partial_T R + \varepsilon^{s+l+1}3b\tau\partial_X\partial_T R = 0.
\end{aligned}
$$

Assuming $s = 3, l = 1$, the following nonlinear partial differential equation is obtained from Eq. (16),

$$
\begin{aligned}
&\varepsilon^2\Big[b + \frac{\rho_c^2 V'(\rho_c)}{\sin^2 \theta_j}\Big]\partial_X R \\
&+ \varepsilon^3\Big[\frac{3b^2\tau}{2} + \frac{(1-2\gamma)\rho_c^2 V'(\rho_c)}{2\sin^2 \theta_j}\Big]\partial_X^2 R \\
&+ \varepsilon^4\Big\{\Big[\frac{(1-6\gamma)\rho_c^2 V'(\rho_c)}{6\sin^2 \theta_j} + \frac{7b^3\tau^2}{6}\Big]\partial_X^3 R \\
&+ \frac{\rho_c^2 V'''(\rho_c)}{6\sin^2 \theta_j}\partial_X R^3 + \partial_T R\Big\} \\
&+ \varepsilon^5\Big\{\Big[\frac{5b^4\tau^3}{8} + \frac{(1-14\gamma)\rho_c^2 V'(\rho_c)}{24\sin^2 \theta_j}\Big]\partial_X^4 R \\
&+ \frac{(1-2\gamma)\rho_c^2 V'''(\rho_c)}{12\sin^2 \theta_j}\partial_X^2 R^3 + 3b\tau\partial_X\partial_T R\Big\} = 0.
\end{aligned}
\tag{17}
$$

Supposing

$$\frac{\tau}{\tau_c} = 1 + \varepsilon^2 \tag{18}$$

for τ near the critical point $(h_c, 1/\tau_c)$, where $\tau_c = \frac{-(1-2\gamma)\sin^2 \theta_j}{3\rho_c^2 V'(\rho_c)}$. Let $b = -\frac{\rho_c^2 V'(\rho_c)}{\sin^2 \theta_j}$, the second- and third-order terms of ε can be eliminated from Eq. (17). Then Eq. (17) can be rewritten as

$$
\begin{aligned}
&\varepsilon^4\Big[\partial_T R - g_1\partial_X^3 R + g_2\partial_X R^3\Big] \\
&+ \varepsilon^5\Big[g_3\partial_X^2 R + g_4\partial_X^2 R^3 + g_5\partial_X^4 R\Big] = 0
\end{aligned}
\tag{19}
$$

where

$$g_1 = -\frac{(1 - 13\gamma - 14\gamma^2)\rho_c^2 V'(\rho_c)}{27\sin^2 \theta_j},$$

$$g_2 = \frac{\rho_c^2 V'''(\rho_c)}{6\sin^2 \theta_j},$$

$$g_3 = -\frac{(1-2\gamma)\rho_c^2 V'(\rho_c)}{2\sin^2 \theta_j},$$

$$g_4 = -\frac{(1-2\gamma)\rho_c^2 V'''(\rho_c)}{12\sin^2 \theta_j},$$

$$g_5 = -\frac{(1 - 6\gamma + 39\gamma^2 + 46\gamma^3)\rho_c^2 V'(\rho_c)}{54\sin^2 \theta_j}.$$

In order to derive the standard MKdV equation with higher-order correction, we make the following transformation in Eq. (19)

$$T_m = -\frac{(1 - 13\gamma - 14\gamma^2)\rho_c^2 V'(\rho_c)}{27 \sin^2 \theta_j} T,$$

$$R_m = 3\sqrt{\frac{V'''(\rho_c)}{(28\gamma^2 + 26\gamma - 2)V'(\rho_c)}} R, \tag{20}$$

with an assumption that

$$1 - 13\gamma - 14\gamma^2 > 0. \tag{21}$$

Then, we obtain the standard MKdV equation with higher-order correction term

$$\partial_{T_m} R_m - \partial_X^3 R_m + \partial_X R_m^3$$
$$+ \frac{\varepsilon}{g_1} \left[g_3 \partial_X^2 R_m \right. \tag{22}$$
$$\left. + \frac{g_1 g_4}{g_2} \partial_X^2 R_m^3 + g_5 \partial_X^4 R_m \right] = 0.$$

If we ignore the $O(\varepsilon)$ term in Eq. (22), it is just the MKdV equation with the kink-antikink solution

$$R_{m0}(X, T_m) = \sqrt{B} \tanh \sqrt{\frac{B}{2}} (X - BT_m). \tag{23}$$

In order to obtain the value of propagation velocity B for the kink-antikink solution, the solvability condition [58–60]

$$(R_{m0}, M[R_{m0}]) \equiv \int_{-\infty}^{\infty} \mathrm{d}X_k R_{m0} M[R_{m0}] = 0 \tag{24}$$

must be satisfied, here $M[R_{m0}]$ is the $O(\varepsilon)$ term in Eq. (22).

$$B = \frac{5g_2 g_3}{2g_2 g_5 - 3g_1 g_4}. \tag{25}$$

Inserting Eq. (20) into Eq. (23), we get the solution of the MKdV equation

$$R(X, T) = \sqrt{\frac{g_1 B}{g_2}} \tanh \sqrt{\frac{B}{2}} (X - Bg_1 T). \tag{26}$$

Then, we gain the kink-antikink solution of the density

$$\rho(j, t) = \rho_c + \sqrt{\frac{g_1 B}{g_2} \left(\frac{\tau}{\tau_c} - 1 \right)} \tanh \left[\sqrt{\frac{B}{2} \left(\frac{\tau}{\tau_c} - 1 \right)} \right.$$
$$\left. \left(j - \frac{\rho_c^2 V'(\rho_c)}{\sin^2 \theta_j} t - Bg_1 \left(\frac{\tau}{\tau_c} - 1 \right) t \right) \right]. \tag{27}$$

And the amplitude C of the kink-antikink solution Eq. (27) is given by

$$C = \sqrt{\frac{g_1 B}{g_2} \left(\frac{\tau}{\tau_c} - 1 \right)}.$$

From the above process, we can find that the kink solution exists only if condition (21) is hold. Hence, the existence condition for kink solution is $\gamma < \frac{1}{14}$. Otherwise, we can not deduce the MKdV Eq. (22). That means the MkdV equation only exists when $\frac{-6 \sin^2 \theta_j}{21 \rho_c^2 V'(\rho_c)} < a < a_c$.

The kink solution represents the coexisting phase, which consists of the freely moving phase with low density and the congested phase with high density. The coexisting curve can be described by $\rho = \rho_c \pm C$. Therefore, we get the coexisting curve in the (ρ, a) plane for $\gamma < \frac{1}{14}$.

In Fig. 1, when $\gamma = 0$, the dash line is the coexisting curve. The coexisting curve and the neutral stability line are similar to the conventional gas–liquid phase transition. Three regions in traffic flow are distinguished: the unstable region which is within the neutral stability line, the metastable region which is between the neutral stability line and the coexisting curve and the stable region which is out of the coexisting curve. When $\gamma = 0.1, 0.2, 0.3$, the condition (22) is not satisfied. Hence, coexisting curves do not exist and are not shown in Fig. 1.

In Fig. 2, the solid lines show the plots of a_c against γ for different θ_j with $\rho_0 = \rho_c = 0.2$, $\mu = 0.3$, $k = 0.14$, $R = 20$. From Fig. 2, the critical sensitivity a_c increases with the increase in γ, which means traffic flow becomes unstable with the increasing of γ. Moreover, the curves a_c represent the phase boundaries between no jam and kink jam for $\gamma < 1/14$ and no jam with chaotic jam for $\gamma \geq 1/14$. For $\gamma \geq 1/14$, the unstable region is further divided into two subregions: kink jam and chaotic jam. The boundary between kink and chaotic jam is the line $a = \frac{7k\sqrt{\mu g R}}{4 \sin^2 \theta_j}$ (dash lines).

Next, we study the nonlinear behavior in the stable and metastable regions, respectively. Firstly, we discuss the triangular shock waves of traffic flow in the stable region. The nonlinear partial differential equation is obtained from Eq. (16) for $s = 2, l = 1$.

$$\varepsilon^2 \left[b + \frac{\rho_0^2 V'(\rho_0)}{\sin^2 \theta_j} \right] \partial_X R$$
$$+ \varepsilon^3 \left\{ \partial_T R + \frac{\rho_0^2 V''(\rho_0)}{2 \sin^2 \theta_j} \partial_X R^2 \right. \tag{28}$$
$$\left. + \left[\frac{3b^2 \tau}{2} + \frac{(1 - 2\gamma)\rho_0^2 V'(\rho_0)}{2 \sin^2 \theta_j} \right] \partial_X^2 R \right\} = 0.$$
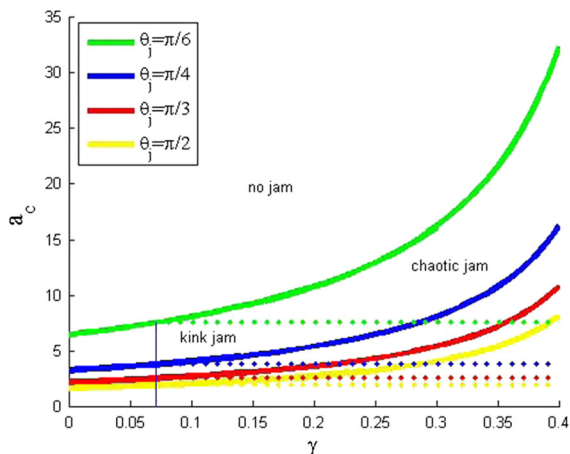
Fig. 2 Phase diagram in the (γ, a) space with $\rho_0 = \rho_c = 0.2$, $R = 20$, $\mu = 0.3$, $k = 0.14$ for different θ_j

Taking $b = -\frac{\rho_0^2 V'(\rho_0)}{\sin^2 \theta_j}$, the second-order term of ε is eliminated in Eq. (28). We obtain the following partial differential equation

$$
\begin{aligned}
&\partial_T R + \frac{\rho_0^2 V''(\rho_0)}{\sin^2 \theta_j} R \partial_X R \\
&= \frac{-(1-2\gamma)\sin^2 \theta_j - 3\rho_0^2 V'(\rho_0)\tau}{2\sin^4 \theta_j} \rho_0^2 V'(\rho_0) \partial_X^2 R.
\end{aligned}
\tag{29}
$$

In accordance with criterion Eq. (13), the coefficient of the second derivative of Eq. (29) is positive in the stable region. Therefore, in the stable region, Eq. (29) is just the Burgers equation. If $R(X, 0)$ is of compact support, then the solution $R(X, T)$ of Eq. (29) is

$$
\begin{aligned}
R(X, T) =\ & \frac{\sin^2 \theta_j}{|\rho_0^2 V''(\rho_0)|T}\left[X - \frac{\eta_{n+1} + \eta_n}{2}\right] \\
& - \frac{\sin^2 \theta_j(\eta_{n+1} - \eta_n)}{2|\rho_0^2 V''(\rho_0)|T} \\
& \tanh\left[\frac{-(1-2\gamma)\sin^2 \theta_j - 3\rho_0^2 V'(\rho_0)\tau}{2\sin^2 \theta_j}\right. \\
& \left. \times V_0'(\rho_0)\frac{(\eta_{n+1} - \eta_n)(X - \xi_n)}{4|V''(\rho_0)|T}\right].
\end{aligned}
\tag{30}
$$

where ξ_n are the coordinates of the shock fronts and η_n are the coordinates of the intersections of the slopes with the x-axis ($n = 1, 2, ..., N$). As $O(\frac{1}{T})$, $R(X, T)$ decays to 0 when $T \to +\infty$. That means any shock wave expressed by Eq. (30) in stable traffic flow region will evolve to a uniform flow when time is sufficient large.

Secondly, we discuss the soliton waves of traffic flow in the metastable region for $\gamma < 1/14$. The nonlinear partial differential equation is obtained from Eq. (16) for $s = 3, l = 2$.

$$
\begin{aligned}
&\varepsilon^3\left[b + \frac{\rho_0^2 V'(\rho_0)}{\sin^2 \theta_j}\right]\partial_X R \\
&+ \varepsilon^4\left[\frac{3b^2\tau}{2} + \frac{(1-2\gamma)\rho_0^2 V'(\rho_0)}{2\sin^2 \theta_j}\right]\partial_X^2 R \\
&+ \varepsilon^5\left\{\partial_T R + \frac{\rho_0^2 V''(\rho_0)}{2\sin^2 \theta_j}\partial_X R^2\right. \\
&\left. + \left[\frac{7b^3\tau^2}{6} + \frac{(1-6\gamma)\rho_0^2 V'(\rho_0)}{6\sin^2 \theta_j}\right]\partial_X^3 R\right\} \\
&+ \varepsilon^6\left\{\frac{(1-2\gamma)\rho_0^2 V''(\rho_0)}{4\sin^2 \theta_j}\partial_X^2 R^2 + 3b\tau\partial_X\partial_T R\right. \\
&\left. + \left[\frac{5b^4\tau^3}{8} + \frac{(1-14\gamma)\rho_0^2 V'(\rho_0)}{24\sin^2 \theta_j}\right]\partial_X^4 R\right\} = 0.
\end{aligned}
\tag{31}
$$

Near the neutral stability line in the unstable region, let

$$
\frac{\tau}{\tau_s} = 1 - \varepsilon^2.
\tag{32}
$$

By taking $b = -\frac{\rho_0^2 V'(\rho_0)}{\sin^2 \theta_j}$, the third- and fourth-order terms of ε are eliminated from Eq. (31), and Eq. (31) can be rewritten as

$$
\begin{aligned}
&\varepsilon^5\left[\partial_T R - f_1\partial_X^3 R - f_2 R\partial_X R\right] \\
&+ \varepsilon^6\left[-f_3\partial_X^2 R + f_4\partial_X^2 R^2 + f_5\partial_X^4 R\right] = 0
\end{aligned}
\tag{33}
$$

where

$$
f_1 = -\frac{(1-13\gamma-14\gamma^2)\rho_0^2 V'(\rho_0)}{27\sin^2 \theta_j},
$$

$$
f_2 = -\frac{\rho_0^2 V''(\rho_0)}{2\sin^2 \theta_j},
$$

$$
f_3 = -\frac{(1-2\gamma)\rho_0^2 V'(\rho_0)}{2\sin^2 \theta_j},
$$

$$
f_4 = -\frac{(1-2\gamma)\rho_0^2 V''(\rho_0)}{4\sin^2 \theta_j},
$$

$$
f_5 = -\frac{(1-6\gamma+39\gamma^2+46\gamma^3)\rho_0^2 V'(\rho_0)}{54\sin^2 \theta_j}.
$$

In order to derive the standard KdV equation with higher-order correction, we make the following transformation in Eq. (33)

$$
T = \sqrt{f_1}T_k,
$$

$$X = -\sqrt{f_1}X_k,$$
$$R = \frac{1}{f_2}R_k. \tag{34}$$

By using Eq. (34), we obtain the standard KdV equation with higher-order correction term

$$\partial_{T_k} R_k + \partial_{X_k}^3 R_k + R_k \partial_{X_k} R_k$$
$$+ \frac{\varepsilon}{\sqrt{f_1}} \left[-f_3 \partial_{X_k}^2 R_k \right.$$
$$\left. + \frac{f_4}{f_2} \partial_{X_k}^2 R_k^2 + \frac{f_5}{f_1} \partial_{X_k}^4 R_k \right] = 0. \tag{35}$$

Next, we assume that $R_k(X_k, T_k) = R_0(X_k, T_k) + \varepsilon R_1(X_k, T_k)$ to consider the $O(\varepsilon)$ correction in Eq. (35). If we ignore the $O(\varepsilon)$ term in Eq. (35), it is just the KdV equation with soliton solutions

$$R_0(X_k, T_k) = A \operatorname{sech}^2 \left[\sqrt{\frac{A}{12}} \left(X_k - \frac{A}{3} T_k \right) \right]. \tag{36}$$

Similar to the process of deriving the value of propagation velocity B for MKdV equation, we obtain the amplitude A for the soliton solution as follows

$$A = \frac{21 f_1 f_2 f_3}{24 f_1 f_4 - 5 f_2 f_5}. \tag{37}$$

Substituting the values of $f_1 - f_5$ into Eq. (37), we get the value of A. Substituting each variable by the original one, we obtain soliton solutions of the density

$$\rho(j, t) = \rho_0 + \frac{A}{f_2} \left(\frac{\tau}{\tau_s} - 1 \right)$$
$$\operatorname{sech}^2 \left[\sqrt{\frac{A}{12 f_1} \left(\frac{\tau}{\tau_s} - 1 \right)} \right.$$
$$\left. \left(j - \frac{\rho_0^2 V'(\rho_0)}{\sin^2 \theta_j} t + \frac{A}{3} \left(\frac{\tau}{\tau_s} - 1 \right) t \right) \right]. \tag{38}$$

Now, we have derived the soliton density wave described by the KdV equation near the neutral stability line.

5 Simulation

In order to check the theoretical results, we carry out numerical simulations in this Section. The initial conditions of the numerical simulation are as follows: There are $N = 100$ lattices in the system, and the periodical boundary condition is applied. The initial perturbations are adopted as follows: $\rho(j, 0) = \rho_0 = \rho_c = 0.2$. The local densities $\rho(N/2, 1)$ and $\rho(N/2 - 1, 1)$ at sites $N/2$ and $N/2 - 1$ at time $t = 1$ are set as 0.15 and 0.25, $k = 0.14$, $R = 20$, $\mu = 0.3$. The radian of the curved road is from $\theta_0 = \pi/4$ to $\theta_N = \pi/3$, where θ_0 and θ_N represent the angle going into and leaving out curved road, respectively.

Figure 3 shows the traffic patterns after a sufficiently long time $t = 100,000$ for different γ with $a = 2.8$. In Fig. 3, the patterns (a)–(d) exhibit the time evolution of the density $\rho(j, t)$ for $\gamma = 0, 0.06, 0.2, 0.4$, respectively. The initial disturbance leads to the kink density waves as shown in patterns (b)–(d). The small amplitude disturbance grows into congested flow since the stability condition is not satisfied. When the stability condition is satisfied, the small amplitude disturbance will dissipate, and traffic flow becomes uniform which is shown in pattern (a). The results show that with the increasing of γ, traffic flow will become unstable and traffic congestion occur. Figure 4 shows the density profile obtained at $t = 90,000$ corresponding to Fig. 3. And it makes us see the evolution of the density with the small disturbances more clearly.

Figure 5 represents the phase space plot of density difference $\rho(j, t) - \rho(j, t - 1)$ against $\rho(t)$ for $t = 60,000s - 70,000s$ at site $j = 1$ corresponding to Fig. 3. For pattern (a) in Fig. 5, the limit cycle leads to a single point which represents the uniform flow in the stable region. The patterns (b)–(d) exhibit the characteristic of periodicity in the form of limit cycle, and the nodes on the right sides as well as on the left sides are corresponding to the traffic states within and out of the kink traffic jam. When $a = 2.8$, the jamming transition occurs among freely moving phase, the coexisting phase with kink density wave and the uniformly congested phase with an increase in the value of γ.

Figures 6, 7 and 8 represent the phase space plot of density difference $\rho(j, t) - \rho(j, t - 1)$ against $\rho(t)$ at site $j = 20, 60, 100$ for $t = 60,000s - 70,000s$ corresponding to Fig. 3, respectively. From Figs. 5c, 6c, 7c and 8c, we can see that compared with other segments of curved road, traffic flow with passing easily becomes unstable and complicated at the entrance and exit of curved road.

Figures 9 and 10 show the hysteresis loop of the flux and velocity for different γ at site $j = 60$ for $t = 60,000s - 70,000s$ corresponding to Fig. 3, respectively. From Fig. 9, it shows that with the decreasing of the value of γ, the size of loops will shrink. When $\gamma = 0$ in Fig. 9a, the stability condition is held, traffic flow is stable, the hysteresis loop will not be gener-
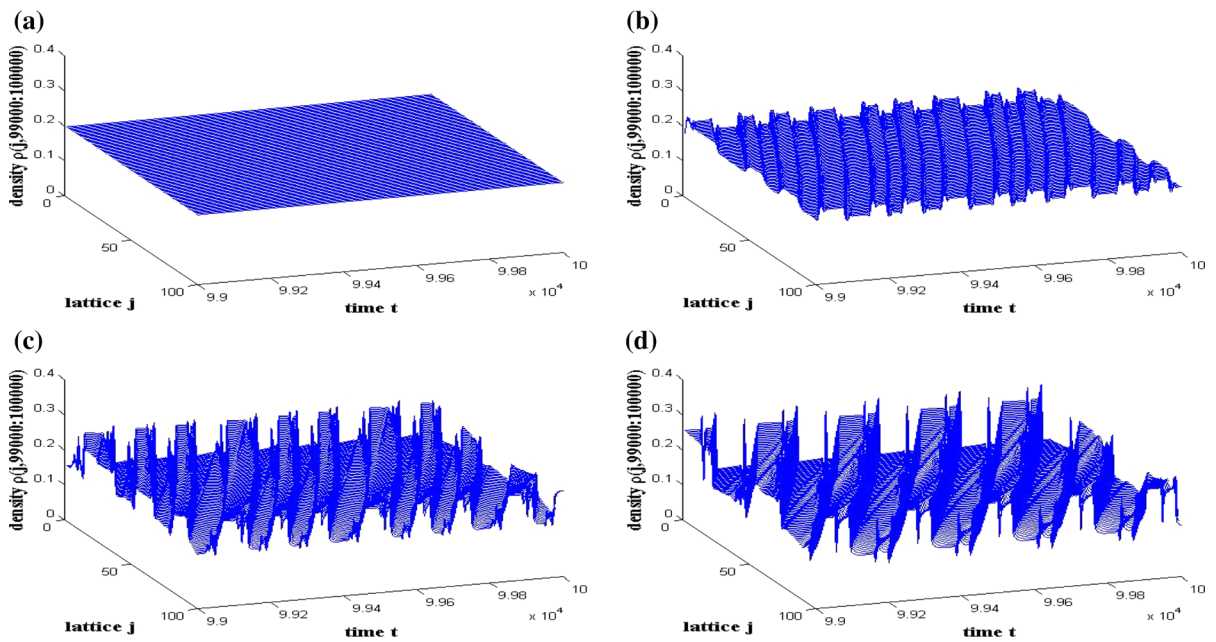
Fig. 3 Traffic patterns from time $t = 99,000$ to $t = 100,000$ with $a = 2.8$, $\rho_0 = \rho_c = 0.2$, $\mu = 0.3$, $k = 0.14$, $\theta_0 = \pi/4$, $\theta_N = \pi/3$ for $\gamma =$ **a** 0, **b** 0.06, **c** 0.2, **d** 0.4, respectively
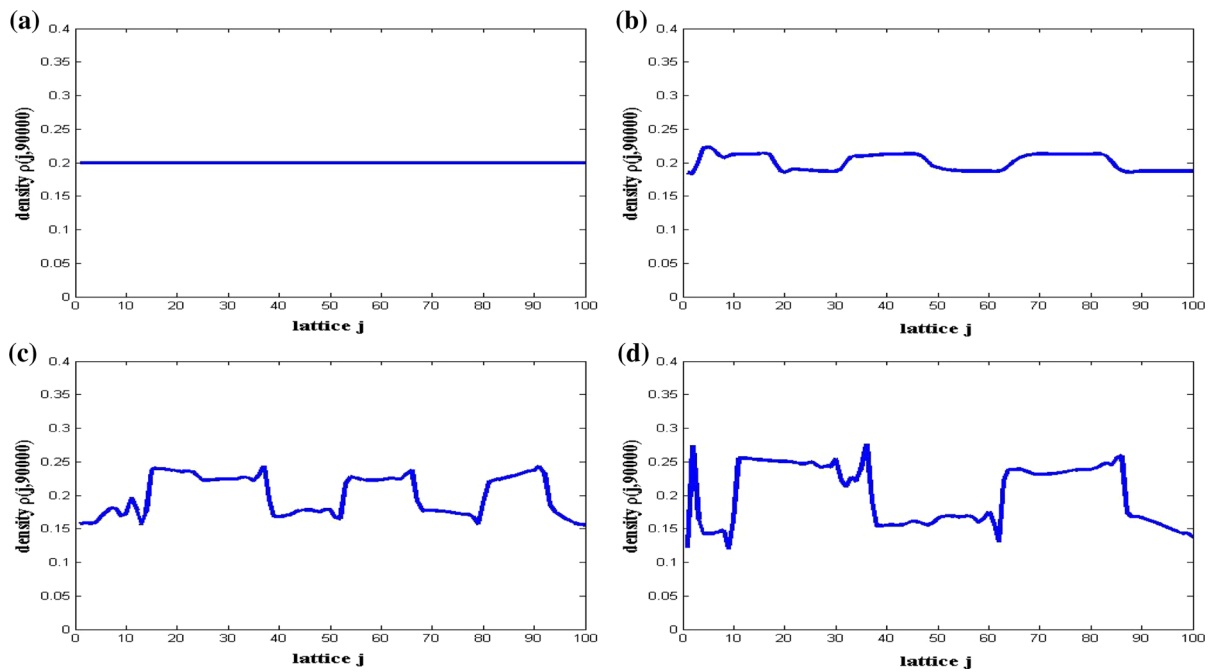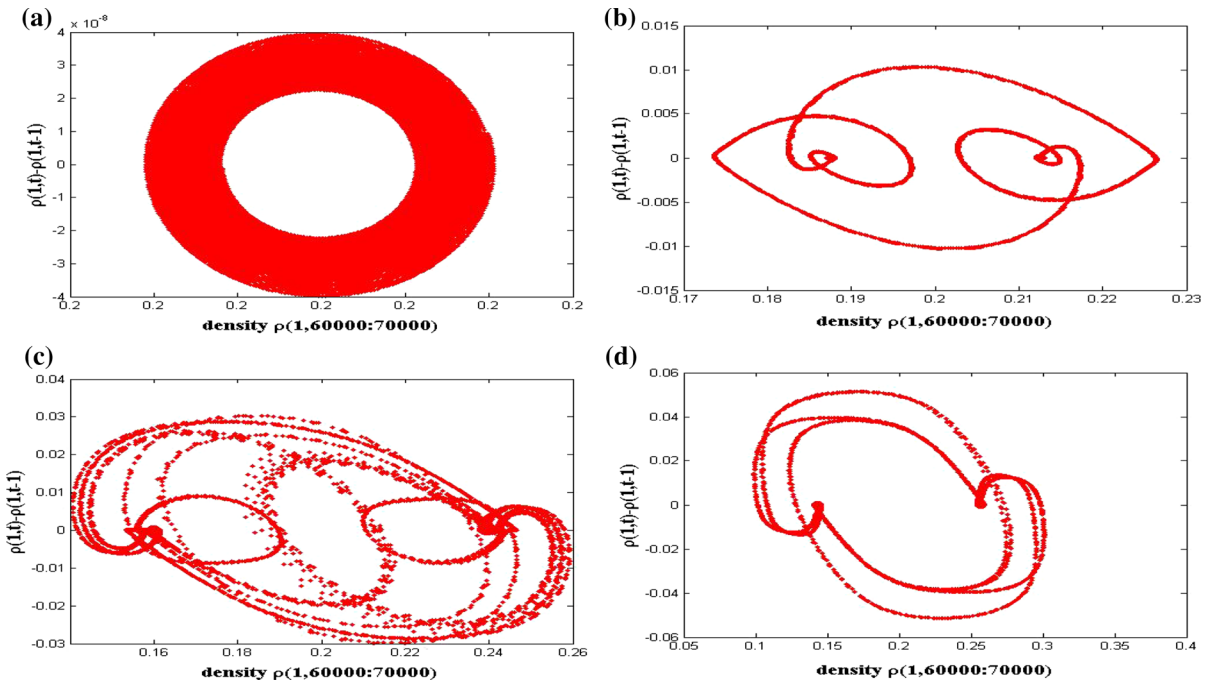

Fig. 4 Density profiles $\rho(j, t)$ at time $t = 90,000$ with $a = 2.8$, $\rho_0 = \rho_c = 0.2$, $\mu = 0.3$, $k = 0.14$, $\theta_0 = \pi/4$, $\theta_N = \pi/3$ for $\gamma =$ **a** 0, **b** 0.06, **c** 0.2, **d** 0.4, respectively
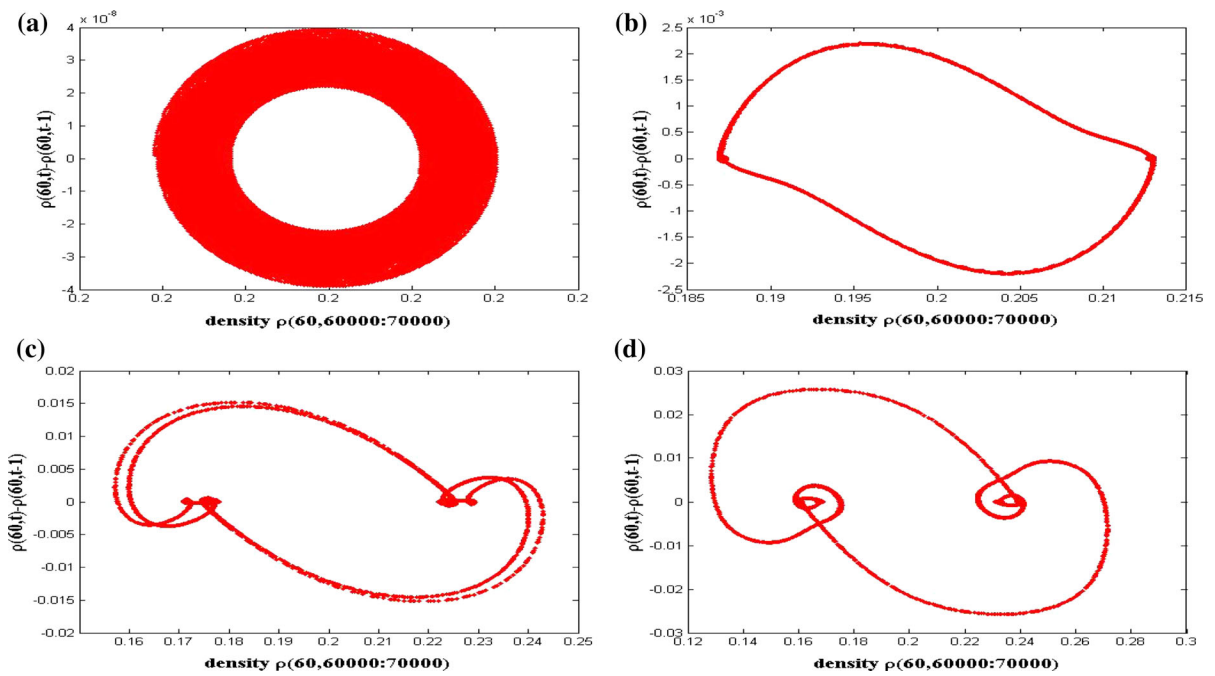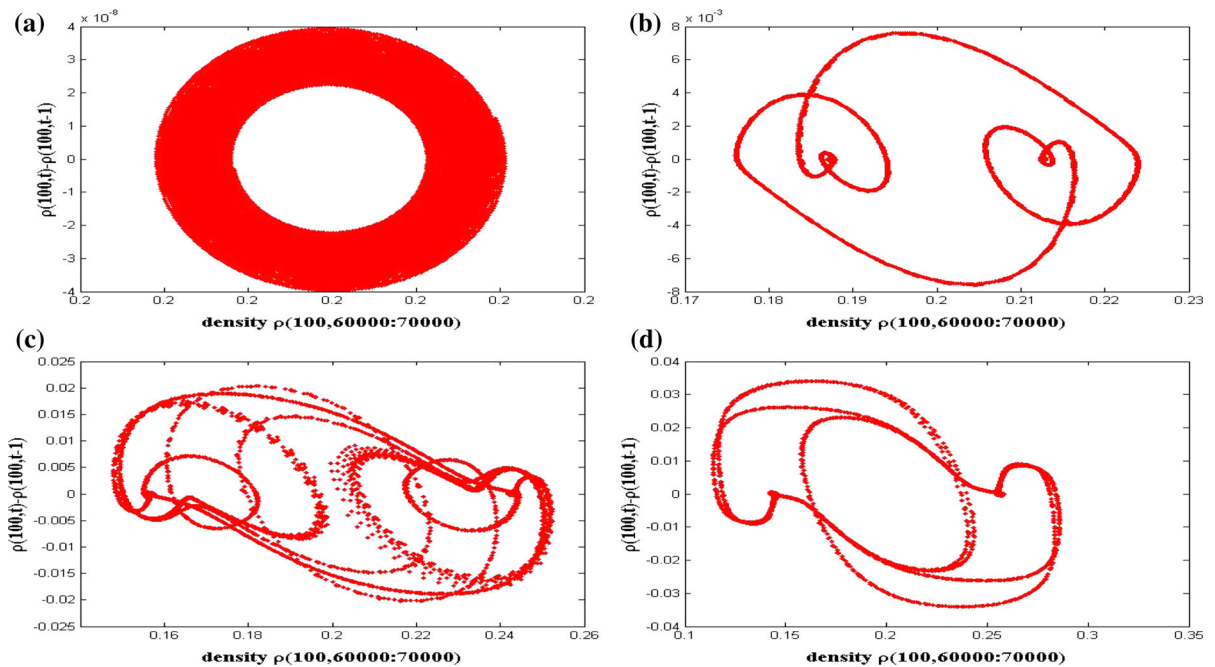
Fig. 5 Phase space plot at site $j = 1$ from time $t = 60,000$ to $t = 70,000$ with $a = 2.8$, $\rho_0 = \rho_c = 0.2$, $\mu = 0.3$, $k = 0.14$, $\theta_0 = \pi/4$, $\theta_N = \pi/3$ for $\gamma =$ **a** 0, **b** 0.06, **c** 0.2, **d** 0.4, respectively
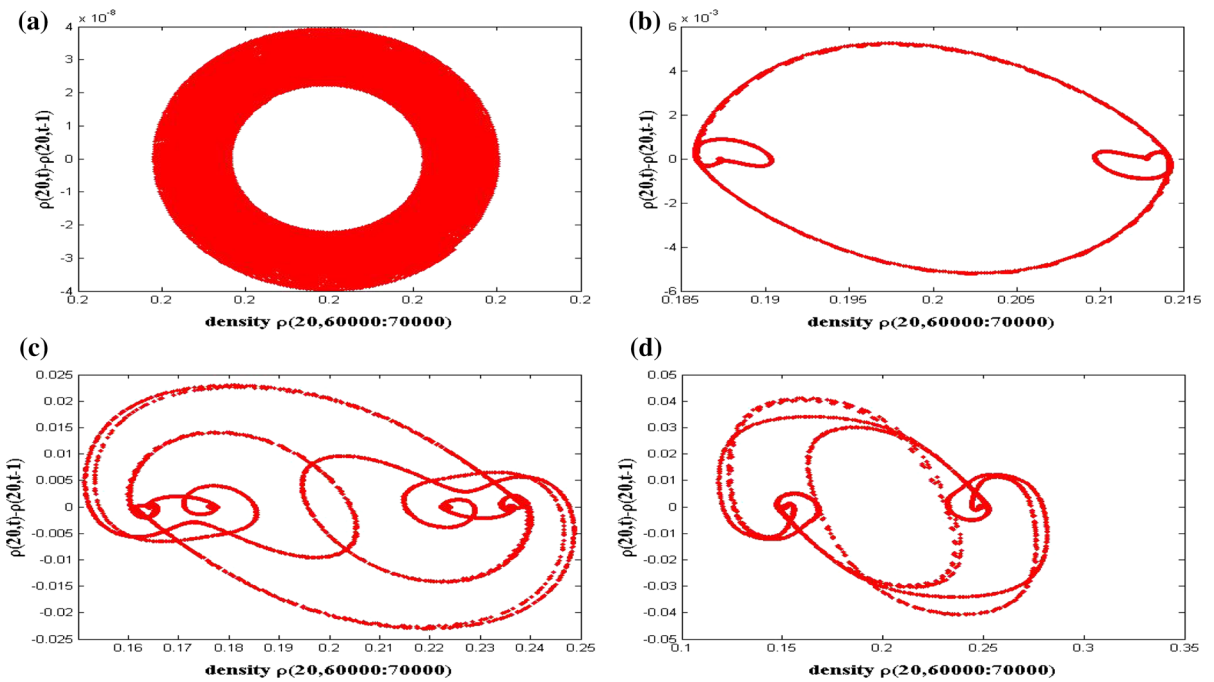
Fig. 6 Phase space plot at site $j = 20$ from time $t = 60,000$ to $t = 70,000$ with $a = 2.8$, $\rho_0 = \rho_c = 0.2$, $\mu = 0.3$, $k = 0.14$, $\theta_0 = \pi/4$, $\theta_N = \pi/3$ for $\gamma =$ **a** 0, **b** 0.06, **c** 0.2, **d** 0.4, respectively
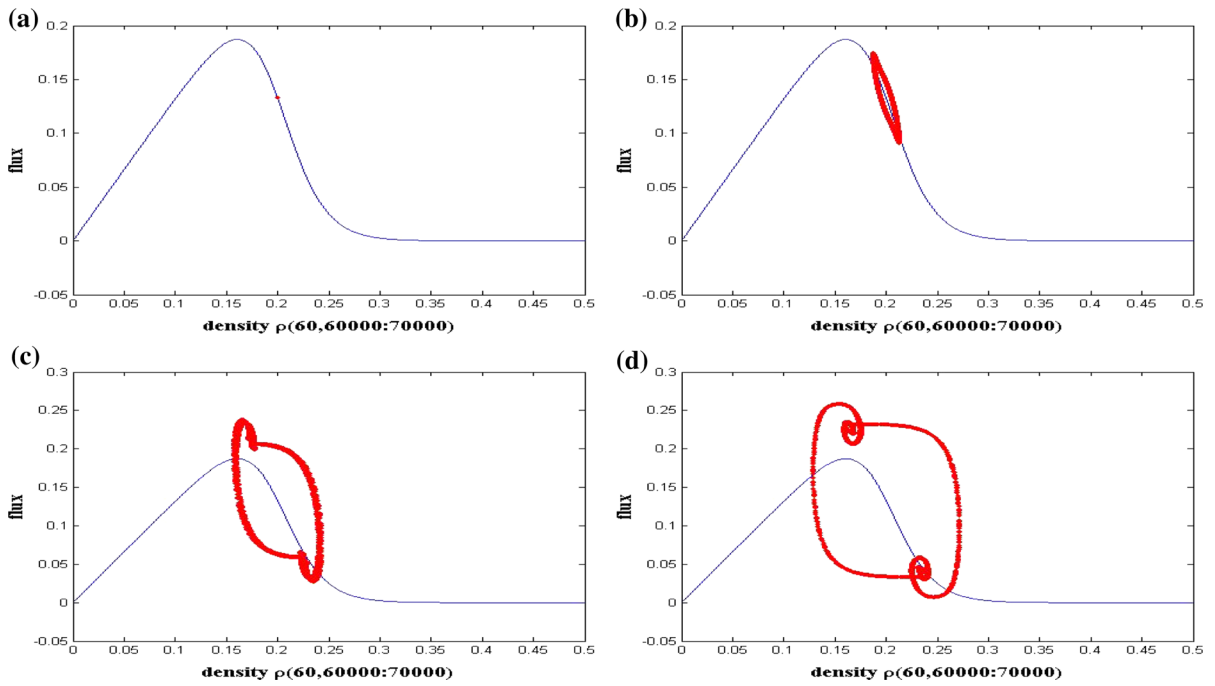
Fig. 7 Phase space plot at site $j = 60$ from time $t = 60,000$ to $t = 70,000$ with $a = 2.8$, $\rho_0 = \rho_c = 0.2$, $\mu = 0.3$, $k = 0.14$, $\theta_0 = \pi/4$, $\theta_N = \pi/3$ for $\gamma =$ **a** 0, **b** 0.06, **c** 0.2, **d** 0.4, respectively

Fig. 8 Phase space plot at site $j = 100$ from time $t = 60,000$ to $t = 70,000$ with $a = 2.8$, $\rho_0 = \rho_c = 0.2$, $\mu = 0.3$, $k = 0.14$, $\theta_0 = \pi/4$, $\theta_N = \pi/3$ for $\gamma =$ **a** 0, **b** 0.06, **c** 0.2, **d** 0.4, respectively
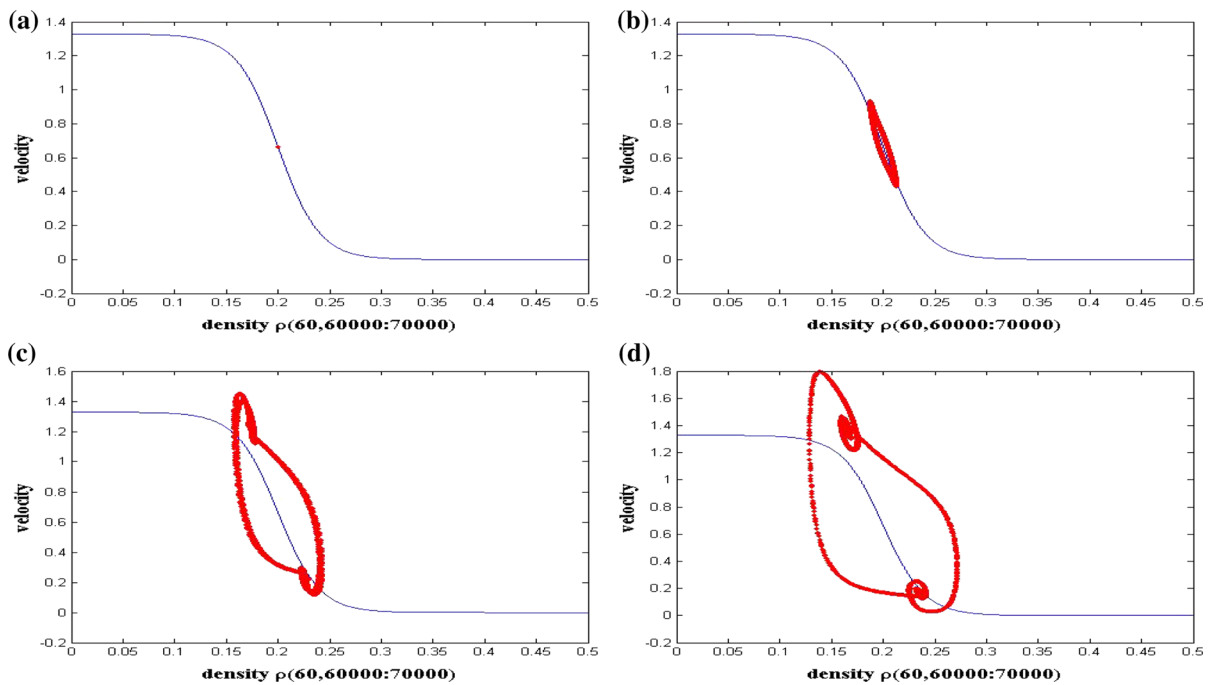
Fig. 9 Hysteresis loop of flux at site $j = 60$ from time $t = 60,000$ to $t = 70,000$ with $a = 2.8$, $\rho_0 = \rho_c = 0.2$, $\mu = 0.3$, $k = 0.14$, $\theta_0 = \pi/4$, $\theta_N = \pi/3$ for $\gamma =$ **a** 0, **b** 0.06, **c** 0.2, **d** 0.4, respectively

Fig. 10 Hysteresis loop of velocity at site $j = 60$ from time $t = 60,000$ to $t = 70,000$ with $a = 2.8$, $\rho_0 = \rho_c = 0.2$, $\mu = 0.3$, $k = 0.14$, $\theta_0 = \pi/4$, $\theta_N = \pi/3$ for $\gamma =$ **a** 0, **b** 0.06, **c** 0.2, **d** 0.4, respectively

ated, and in phase space, there will be only a point on the optimal current curve instead. From Fig. 10, it shows that with the increasing of the value of γ, the size of loops will expand. When $\gamma = 0$ in Fig. 10a, the stability condition is held, the traffic flow is stable, the hysteresis loop will not be generated, and in phase space, there will be only a point on the optimal velocity curve instead.

Figure 11 shows the traffic patterns after a sufficiently long time $t = 100,000$ for different γ with $a = 3.5$. In Fig. 11, the patterns (a)–(d) exhibit the time evolution of the density $\rho(j,t)$ for $\gamma = 0, 0.06, 0.2, 0.4$, respectively. When the stability condition is satisfied, the small amplitude disturbance will dissipate and traffic flow becomes uniform which is shown in patterns (a) and (b). For patterns (c) and (d), the stability condition is not satisfied; hence, the traffic flow is unstable due to the initial disturbance. Furthermore, we can see the traffic patterns in Fig. 11c, d are different from the ones in Fig. 3b–d. In Fig. 11c, d, the density waves band with one another, break up and propagates in the backward direction. The main reason is that $a \geq \frac{7k\sqrt{\mu g R}}{4\sin^2\theta_j}$, which means the traffic is in chaotic jam phase; hence, traffic flow becomes chaotic. Figure 12 shows the density profile obtained at $t = 90,000$ corresponding to Fig. 11.

Figure 13 represents the phase space plot of density difference $\rho(j,t) - \rho(j,t-1)$ against $\rho(t)$ for $t = 60,000s - 70,000s$ at site $j = 1$ corresponding to Fig. 11. For patterns (a) and (b), the uniform flow in the stable region is represented by a single point. Patterns (c) and (d) exhibit the behavior characteristics of chaos; the patterns exhibit dispersed plots around a closed loop due to the irregular traffic waves. This is the characteristics of chaos.

Figures 14, 15 and 16 represent the phase space plot of density difference $\rho(j,t) - \rho(j,t-1)$ against $\rho(t)$ at site $j = 20, 60, 100$ for $t = 60,000s - 70,000s$ corresponding to Fig. 11, respectively. From Figs. 13d, 14d, 15d and 16d, we can see that compared with other segments of curved road, traffic flow with passing easily becomes unstable at the entrance and exit of curved road, especially the entrance of curved road.

Figures 17 and 18 show the hysteresis loop of the flux and velocity for different γ at site $j = 60$ for $t = 60,000s - 70,000s$ corresponding to Fig. 11, respectively. From Fig. 17, it shows that with the decreasing of the value of γ, the size of loops will shrink. When $\gamma = 0, 0.06$ in Fig. 17a, b, the stability condition is held, traffic flow is stable, the hysteresis loop will not be generated, and in phase space, there will be only a point on the optimal current curve instead. When $\gamma = 0.2, 0.4$, the hysteresis loops exhibit the behavior characteristics of chaos. From Fig. 18, it shows that with the increasing of the value of γ, the size of loops will be expansion. When $\gamma = 0, 0.06$ in Fig. 18a, b, the stability condition is held, the traffic flow is stable, and in phase space, there will be only a point on the optimal velocity curve instead. When $\gamma = 0.2, 0.4$, the hysteresis loops exhibit dispersed plots around a closed loop due to the irregular traffic behavior. This is the characteristics of chaos.

Moreover, From Figs. 3c and 11c (Figs. 3d, 11d), we can see that for constant γ which is larger than the critical value, the instable region is divided into kink region and chaotic region. And the congested flow occurs from chaotic jam to kink jam with decreasing sensitivity a.

6 Summary

In order to investigate the effect of passing on traffic flow on curved road, we propose an extended lattice hydrodynamic model for traffic flow on curved road by taking passing into account. We obtain the stability condition of the proposed model by the use of linear stability theory. The stability condition shows that passing behavior play an important role in influencing the stability of traffic flow. The nonlinear wave equations including Burgers, KdV and MKdV are obtained to describe traffic flow behavior in different regions, respectively. The analytical and simulation results show that reducing passing behavior may enhance the stability of traffic flow. Jamming transition occurs between uniform flow and kink jam when γ is less than the critical value. When γ is larger than the critical value, jamming transition occurs from uniform flow to irregular wave through chaotic phase with decreasing sensitivity a. In addition, compared with other segments of curved road, traffic flow with passing easily becomes unstable and complicated at the entrance and exit of curved road, especially at the entrance of curved road. Such findings mean that at the entrance and exit of curved road, passing behavior should be prohibited. As to other segments
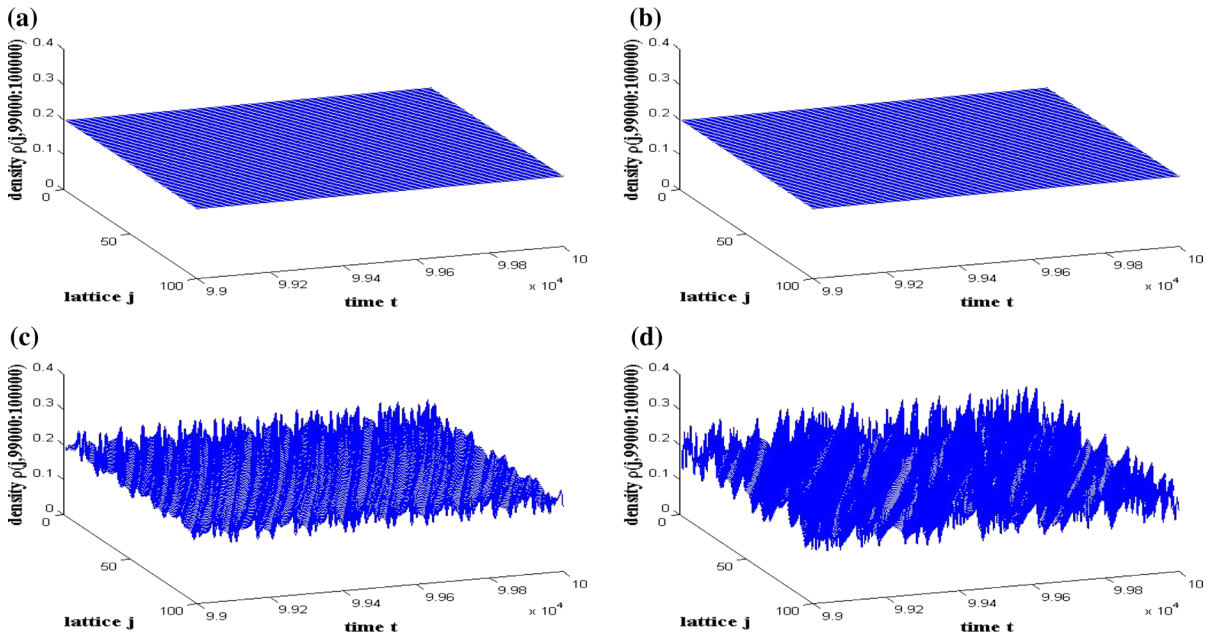
(a)

(b)

(c)

(d)

Fig. 11 Traffic patterns from time $t = 99,000$ to $t = 100,000$ with $a = 3.5$, $\rho_0 = \rho_c = 0.2$, $\mu = 0.3$, $k = 0.14$, $\theta_0 = \pi/4$, $\theta_N = \pi/3$ for $\gamma = $ **a** 0, **b** 0.06, **c** 0.2, **d** 0.4, respectively
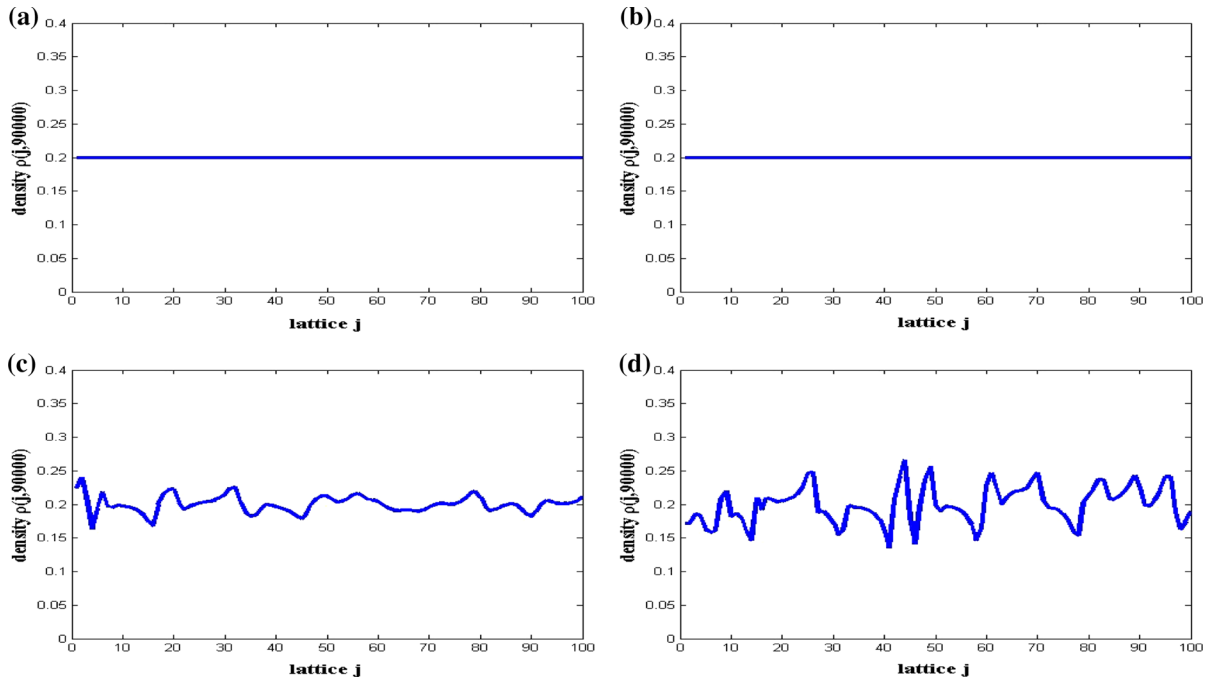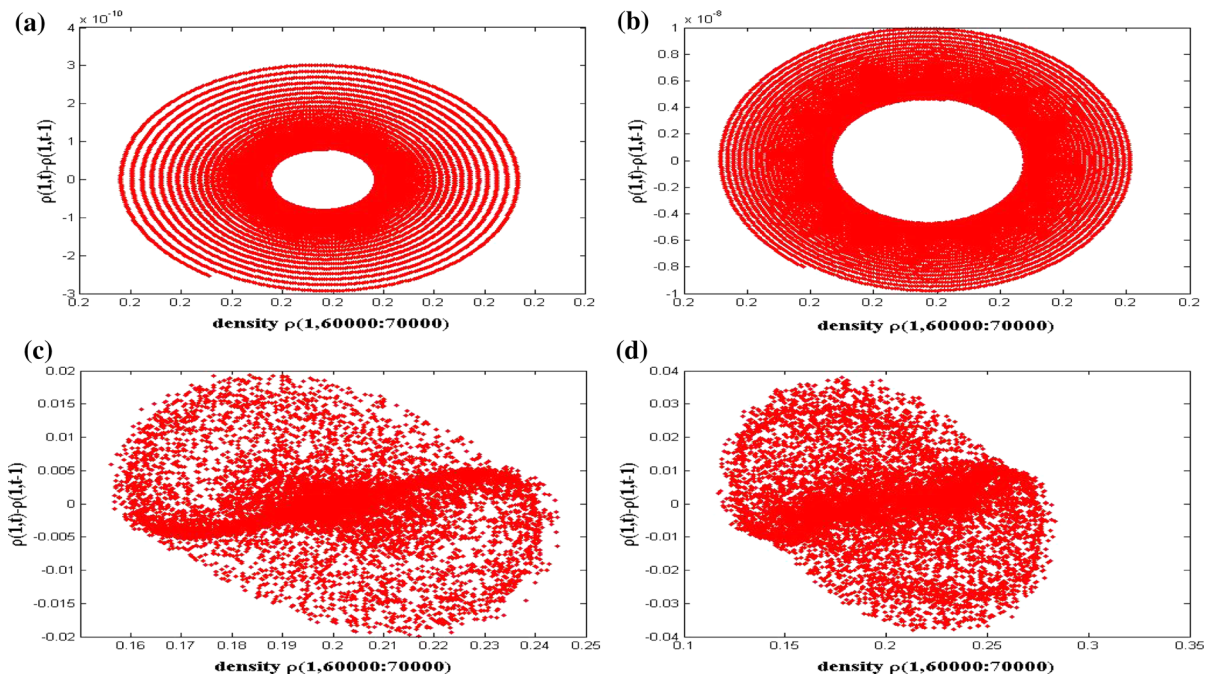
(a)

(b)

(c)

(d)

Fig. 12 Density profiles $\rho(j, t)$ at time $t = 90,000$ with $a = 3.5$, $\rho_0 = \rho_c = 0.2$, $\mu = 0.3$, $k = 0.14$, $\theta_0 = \pi/4$, $\theta_N = \pi/3$ for $\gamma = $ **a** 0, **b** 0.06, **c** 0.2, **d** 0.4, respectively
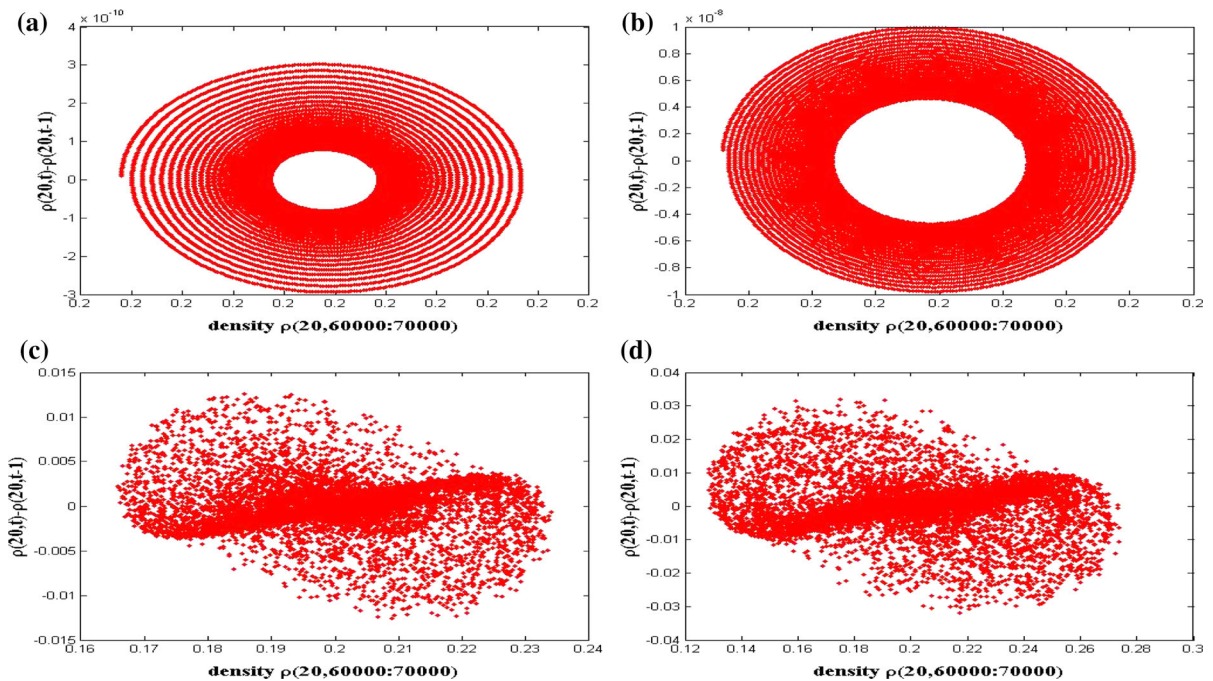
Fig. 13 Phase space plot at site $j = 1$ from time $t = 60,000$ to $t = 70,000$ with $a = 3.5$, $\rho_0 = \rho_c = 0.2$, $\mu = 0.3$, $k = 0.14$, $\theta_0 = \pi/4$, $\theta_N = \pi/3$ for $\gamma = $ **a** 0, **b** 0.06, **c** 0.2, **d** 0.4, respectively
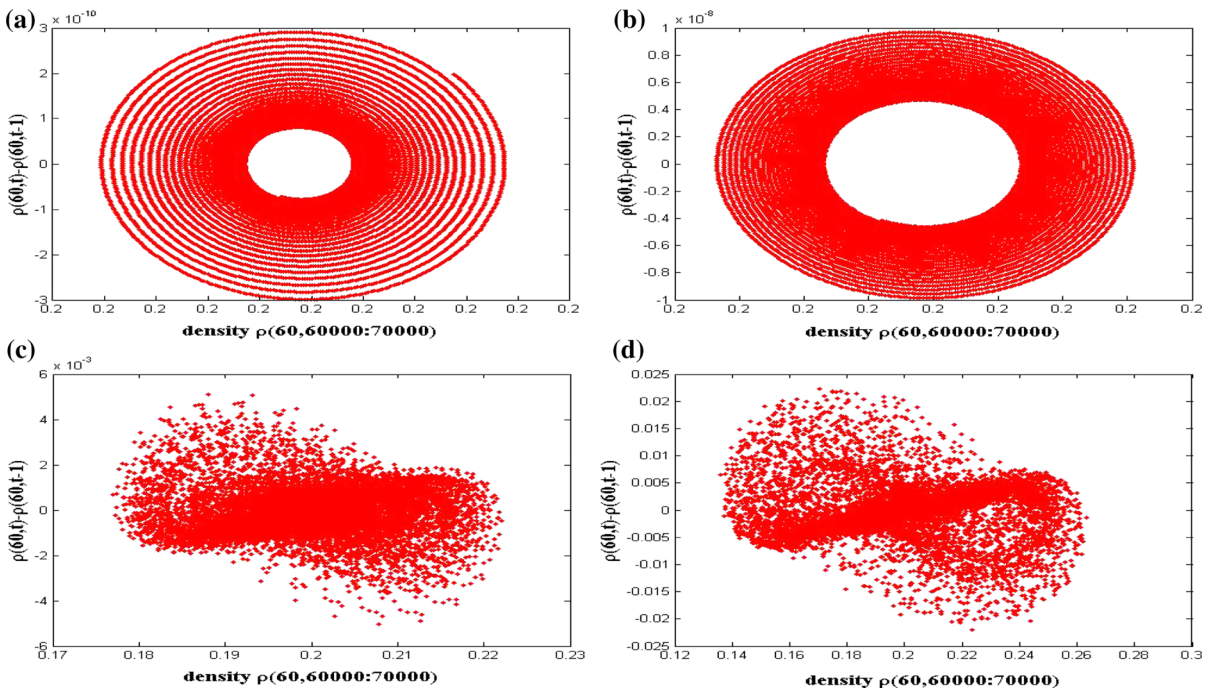

Fig. 14 Phase space plot at site $j = 20$ from time $t = 60,000$ to $t = 70,000$ with $a = 3.5$, $\rho_0 = \rho_c = 0.2$, $\mu = 0.3$, $k = 0.14$, $\theta_0 = \pi/4$, $\theta_N = \pi/3$ for $\gamma = $ **a** 0, **b** 0.06, **c** 0.2, **d** 0.4, respectively

Fig. 15 Phase space plot at site $j = 60$ from time $t = 60,000$ to $t = 70,000$ with $a = 3.5$, $\rho_0 = \rho_c = 0.2$, $\mu = 0.3$, $k = 0.14$, $\theta_0 = \pi/4$, $\theta_N = \pi/3$ for $\gamma = $ **a** 0, **b** 0.06, **c** 0.2, **d** 0.4, respectively
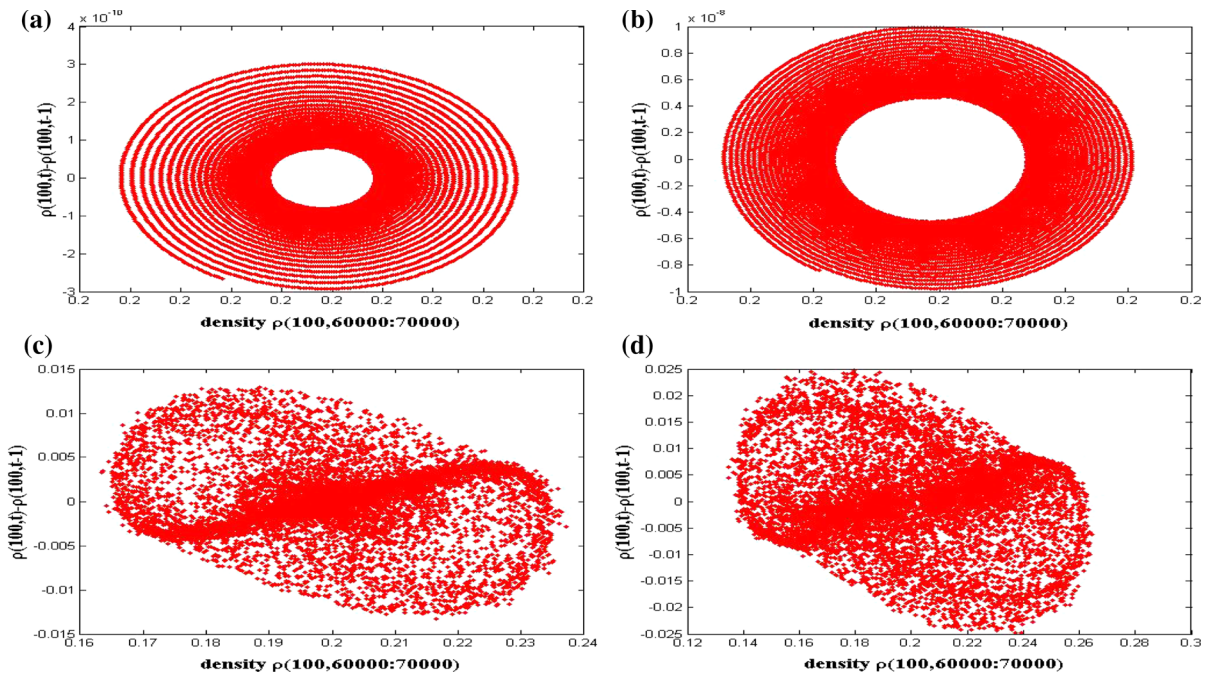

Fig. 16 Phase space plot at site $j = 100$ from time $t = 60,000$ to $t = 70,000$ with $a = 3.5$, $\rho_0 = \rho_c = 0.2$, $\mu = 0.3$, $k = 0.14$, $\theta_0 = \pi/4$, $\theta_N = \pi/3$ for $\gamma = $ **a** 0, **b** 0.06, **c** 0.2, **d** 0.4, respectively
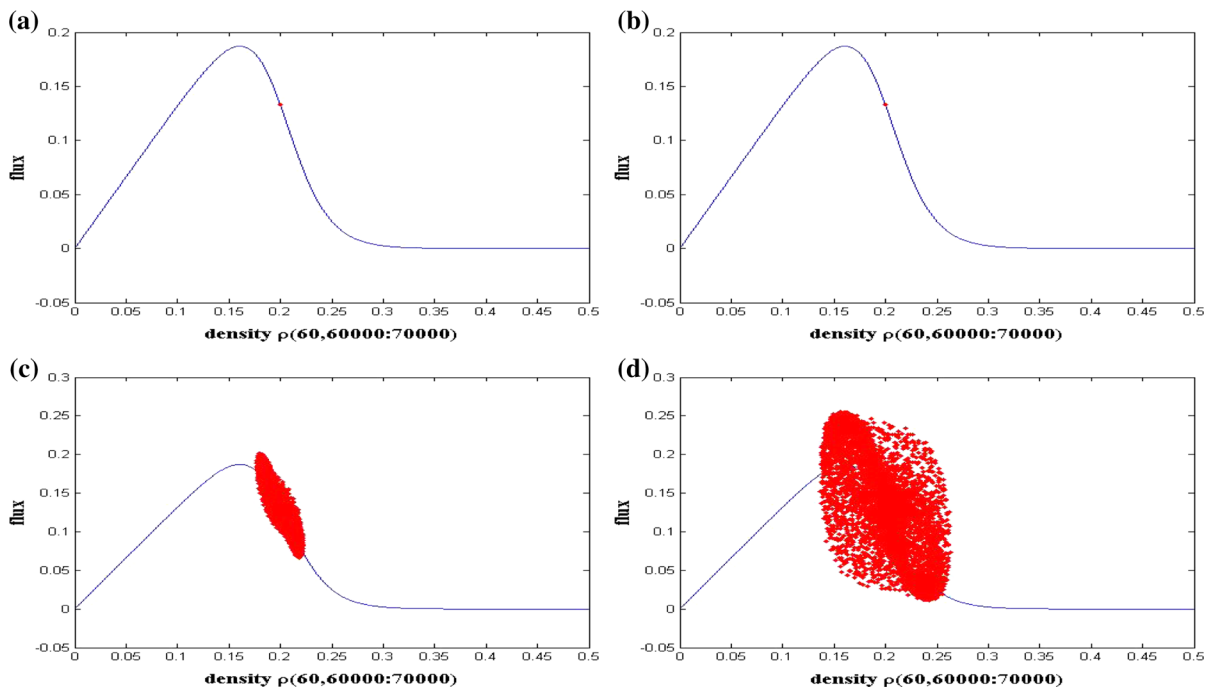
Fig. 17 Hysteresis loop of flux at site $j = 60$ from time $t = 60,000$ to $t = 70,000$ with $a = 3.5$, $\rho_0 = \rho_c = 0.2$, $\mu = 0.3$, $k = 0.14$, $\theta_0 = \pi/4$, $\theta_N = \pi/3$ for $\gamma =$ **a** 0, **b** 0.06, **c** 0.2, **d** 0.4, respectively
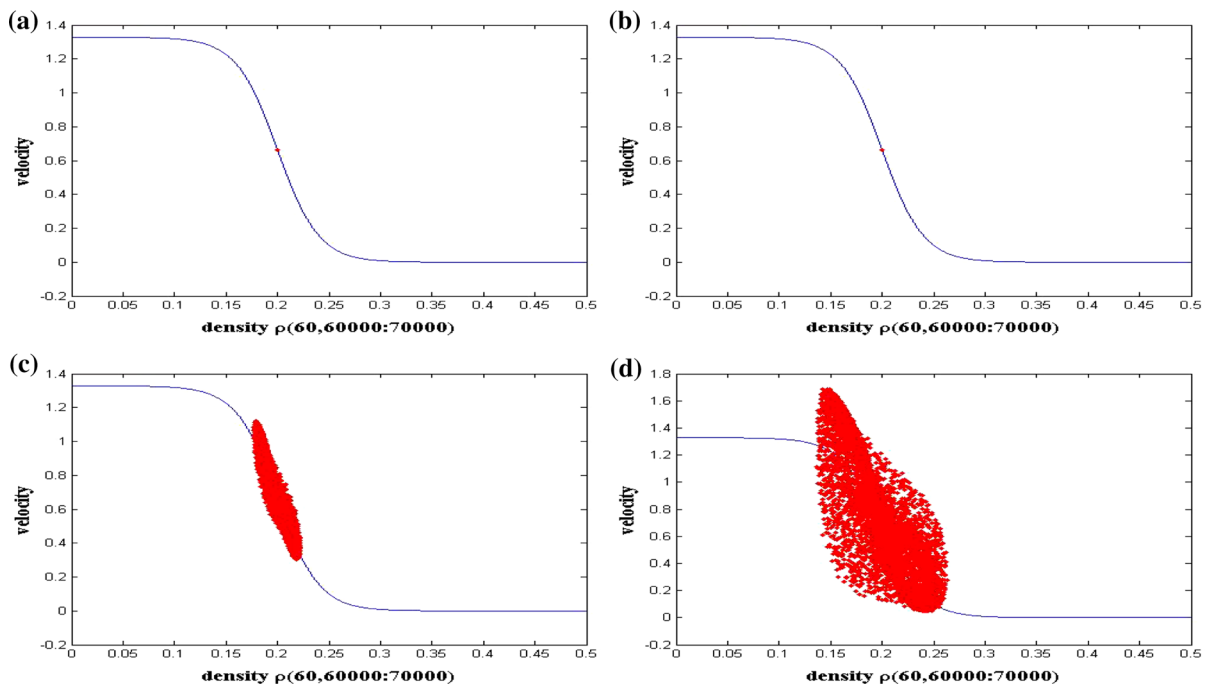

Fig. 18 Hysteresis loop of velocity at site $j = 60$ from time $t = 60,000$ to $t = 70,000$ with $a = 3.5$, $\rho_0 = \rho_c = 0.2$, $\mu = 0.3$, $k = 0.14$, $\theta_0 = \pi/4$, $\theta_N = \pi/3$ for $\gamma =$ **a** 0, **b** 0.06, **c** 0.2, **d** 0.4, respectively

of curved road, when passing conditions are satisfied, passing behavior could be taken if necessary.

References

1. Helbing, D.: Traffic and related self-driven many-particle systems. Rev. Mod. Phys. **73**(4), 1067–1141 (2001)
2. Nagatani, T.: The physics of traffic jams. Rep. Prog. Phys. **65**, 1331–1386 (2002)
3. Schadschneider, A.: Traffic flow: a statistical physics point of view. Phys. A **313**, 1–40 (2002)
4. Schadschneider, A., Chowdhury, D., Nishinari, K.: Stochastic Transport in Complex Systems-From Molecules to Vehicles. Elsevier, Amsterdam (2010)
5. Kurtze, D.A., Hong, D.C.: Traffic jams, granular flow, and soliton selection. Phys. Rev. E **52**(1), 218–221 (1995)
6. Gupta, A.K., Katiyar, V.K.: Analyses of shock waves and traffic jams in traffic flow. J. Phys. A: Math. Gen. **38**, 4069–4083 (2005)
7. Gupta, A.K., Katiyar, V.K.: Phase transition of traffic states with an on-ramp. Phys. A **371**(2), 674–682 (2006)
8. Gupta, A.K., Katiyar, V.K.: A new anisotropic continuum model for traffic flow. Phys. A **368**(2), 551–559 (2006)
9. Gupta, A.K., Sharma, S.: Nonlinear analysis of traffic jams in an anisotropic continuum model. Chin. Phys. B **19**(11), 110503 (2010)
10. Gupta, A.K., Sharma, S.: Analysis of wave properties of a new two-lane continuum model with consideration of the coupling effect. Chin. Phys. B **21**(1), 015201 (2012)
11. Gupta, A.K.: A section approach to a traffic flow model on networks. Int. J. Mod. Phys. C **25**(4), 1350018 (2013)
12. Gupta, A.K., Dhiman, I.: Analyses of a continuum traffic flow model for a non-lane-based system. Int. J. Mod. Phys. C **25**(9), 1450045 (2014)
13. Gupta, A.K., Dhiman, I.: Phase diagram of a continuum traffic flow model with a static bottleneck. Nonlinear Dyn. **79**(1), 663–671 (2014)
14. Kerner, B.S., Konhauser, P.: Cluster effect in initially homogeneous traffic flow. Phys. Rev. E **48**(4), 2335–2338 (1993)
15. Kerner, B.S., Klenov, S.L., Hiller, A.: Empirical test of a microscopic three-phase traffic theory. Nonlinear Dyn. **49**(4), 525–553 (2007)
16. Del Castillo, J.M., Benitez, F.G.: On the functional form of the speed-density relationship-I: general theory. Transp. Res. B **29**(5), 373–389 (1995)
17. Boer, E.R.: Car following from the driver's perspective. Transp. Res. F **2**, 201–206 (1999)
18. Treiber, M., Hennecke, A., Helbing, D.: Congested traffic states in empirical observations and microscopic simulations. Phys. Rev. E **62**(2), 1805–1824 (2000)
19. Treiber, M., Kesting, A., Helbing, D.: Delays, inaccuracies, and anticipation in microscopic traffic models. Phys. A **360**, 71–88 (2006)
20. Jiang, R., Wu, Q.S., Zhu, Z.J.: Full velocity difference model for a car-following theory. Phys. Rev. E **64**(1), 017101 (2001)
21. Xue, Y., Dong, L.Y., Yuan, Y.W., Dai, S.Q.: The effect of the relative velocity on traffic flow. Commun. Theor. Phys. **38**(2), 230–234 (2002)
22. Yu, L., Li, T., Shi, Z.K.: Density waves in a traffic flow with reaction-time delay. Phys. A **389**, 2607–2616 (2010)
23. Ge, H.X., Cheng, R.J., Dai, S.Q.: KdV and kink-antikink solitons in car-following models. Phys. A **357**, 466–476 (2005)
24. Tang, T.Q., Wang, Y.P., Yang, X.B., Wu, Y.H.: A new car-following model accounting for varying road condition. Nonlinear Dyn. **70**(2), 1397–1405 (2012)
25. Tang, T.Q., Huang, H.J., Zhao, S.G., Xu, G.: An extended OV model with consideration of driver's memory. Int. J. Mod. Phys. B **23**(5), 743–752 (2009)
26. Tang, T.Q., Huang, H.J., Wong, S.C., Jiang, R.: A car following model with the anticipation effect of potential lane changing. Acta Mech. Sin. **24**, 399–407 (2008)
27. Zhou, J., Shi, Z.K., Cao, J.L.: Nonlinear analysis of the optimal velocity difference model with reaction-time delay. Phys. A **396**, 77–87 (2014)
28. Zhou, J., Shi, Z.K., Cao, J.L.: An extended traffic flow model on a gradient highway with the consideration of the relative velocity. Nonlinear Dyn. **78**, 1765–1779 (2014)
29. Zhou, J.: An extended visual angle model for car-following theory. Nonlinear Dyn. **81**(1), 549–560 (2015)
30. Zhou, J., Shi, Z.K.: A modified full velocity difference model withthe consideration of velocity deviation. Int. J. Mod. Phys. C **27**(6), 1650069 (2016)
31. Nagatani, T., Nakanishi, K.: Delay effect on phase transitions in traffic dynamics. Phys. Rev. E **57**(6), 6415–6421 (1998)
32. Lee, H.K., Lee, H.W., Kim, D.: Steady-state solutions of hydrodynamic traffic models. Phys. Rev. E **69**(1), 016118 (2004)
33. Nagatani, T.: Modified KdV equation for jamming transition in the continuum models of traffic. Phys. A **271**, 599–607 (1998)
34. Nagatani, T.: Jamming transition in a two-dimensional traffic flow model. Phys. Rev. E **59**, 4857–4864 (1999)
35. Nagatani, T.: Jamming transition of high-dimensional traffic dynamics. Phys. A **272**, 592–611 (1999)
36. Nagatani, T.: Jamming transition in traffic flow on triangular lattice. Phys. A **271**, 200–221 (1999)
37. Nagatani, T.: Chaotic jam and phase transition in traffic flow with passing. Phys. Rev. E **60**(2), 1535–1541 (1999)
38. Gupta, A.K., Redhu, P.: Analyses of the driver's anticipation effect in a new lattice hydrodynamic traffic flow model with passing. Nonlinear Dyn. **76**, 1001–1011 (2014)
39. Gupta, A.K., Sharma, S., Redhu, P.: Effect of multi-phase optimal velocity function on jamming transition in a lattice hydrodynamic model with passing. Nonlinear Dyn. **80**(3), 1091–1108 (2015)

40. Sharma, S.: Modeling and analyses of driver's characteristics in a traffic system with passing. Nonlinear Dyn. **86**, 2093–2104 (2016)

41. Redhu, P., Gupta, A.K.: Jamming transitions and the effect of interruption probability in a lattice traffic flow model with passing. Phys. A **421**, 249–260 (2015)

42. Gupta, A.K., Redhu, P.: Analyses of driver's anticipation effect in sensing relative flux in a new lattice model for two-lane traffic system. Phys. A **392**, 5622–5632 (2013)

43. Sharma, S.: Effect of driver's anticipation in a new two-lane lattice model with the consideration of optimal current difference. Nonlinear Dyn. **81**, 991–1003 (2015)

44. Redhu, P., Gupta, A.K.: Effect of forward looking sites on a multi-phase lattice hydrodynamic model. Phys. A **445**, 150–160 (2016)

45. Redhu, P., Gupta, A.K.: Delayed-feedback control in a Lattice hydrodynamic model. Commun. Nonlinear Sci. Numer. Simul. **27**, 263–270 (2015)

46. Gupta, A.K., Sharma, S., Redhu, P.: Analyses of lattice traffic flow model on a gradient highway. Commun. Theor. Phys. **62**, 393–404 (2014)

47. Gupta, A.K., Redhu, P.: Analyses of a modified two-lane lattice model by considering the density difference effect. Commun. Nonlinear Sci. Numer. Simul. **19**(5), 1600–1610 (2014)

48. Peng, G.H.: A new lattice model of the traffic flow with the consideration of the driver anticipation effect in a two-lane system. Nonlinear Dyn. **73**, 1035–1043 (2013)

49. Peng, G.H., Cai, X.H., Liu, C.Q., Tuo, M.X.: A new lattice model of traffic flow with the anticipation effect of potential lane changing. Phys. Lett. A **376**, 447–451 (2012)

50. Peng, G.H., Cai, X.H., Liu, C.Q., Cao, B.F.: A new lattice model of traffic flow with the consideration of the driver's forecast effects. Phys. Lett. A **375**, 2153–2157 (2011)

51. Peng, G.H., He, H.D., Lu, W.Z.: A new lattice model with the consideration of the traffic interruption probability for two-lane traffic flow. Nonlinear Dyn. **81**(1), 417–424 (2015)

52. Peng, G.H., Cai, X.H., Cao, B.F., Liu, C.Q.: Non-lane-based lattice hydrodynamic model of traffic flow considering the lateral effects of the lane width. Phys. Lett. A **375**, 2823–2827 (2011)

53. Zhang, M., Sun, D.H., Tian, C.: An extended two-lane traffic flow lattice model with driver's delay time. Nonlinear Dyn. **77**, 839–847 (2014)

54. Zhang, G., Sun, D.H., Liu, W.N., Zhao, M., Chen, S.L.: Analysis of two-lane lattice hydrodynamic model with consideration of drivers' characteristics. Phys. A **422**, 16–24 (2015)

55. Wang, T., Gao, Z.Y., Zhang, W.Y., Zhang, J., Li, S.B.: Phase transitions in the two-lane density difference lattice hydrodynamic model of traffic flow. Nonlinear Dyn. **77**, 635–642 (2014)

56. Wang, T., Gao, Z.Y., Zhang, J.: Stabilization effect of multiple density difference in the lattice hydrodynamic model. Nonlinear Dyn. **73**, 2197–2205 (2013)

57. Ge, H.X., Cheng, R.J.: The "backward looking" effect in the lattice hydrodynamic model. Phys. A **387**, 6952–6958 (2008)

58. Tang, T.Q., Huang, H.J., Xue, Y.: An improved two-lane traffic flow lattice model. Acta Phys. Sin. **55**, 4026–4031 (2006)

59. Zhu, W.X., Zhang, L.D.: Friction coefficient and radius of curvature effects upon traffic flow on a curved Road. Phys. A **391**, 4597–4605 (2012)

60. Zhu, W.X., Zhang, L.D.: A novel lattice traffic flow model and its solitary density waves. Int. J. Mod. Phys. C **23**(3), 1250025 (2012)

61. Cao, J.L., Shi, Z.K.: A novel lattice traffic flow model on a curved road. Int. J. Mod. Phys. C **26**(11), 1550121 (2015)

62. Zhou, J., Shi, Z.K.: Lattice hydrodynamic model for traffic flow on curved road. Nonlinear Dyn. **83**(3), 1217–1236 (2016)